Aalto University School of Engineering
CFD-group/ Department of Applied Mechanics

MEMO No CFD/MECHA-23-2012 DATE: November 15, 2012

TITLE

The Effect of Free-Stream Turbulence Parameters on the SST $k-\omega$ Turbulence Model on a Flow over a Flat Plate

AUTHOR(S)
Juhaveikko Ala-Juusela and Timo Siikonen

ABSTRACT

An assessment of the SST $k-\omega$ turbulence model is made using different free-stream values for k and ω. A flow over a flat plate at high Reynolds numbers is used as a test case.

MAIN RESULT

A modification to reduce the effect of free-stream turbulence quantities on the SST $k-\omega$ turbulence model is tested. It is found out that the method in some situations removed the effect of the free-stream values, but is not as effective at high Reynolds numbers.

PAGES
24

KEY WORDS
A flat-plate flow, CFD, turbulence, SST $k-\omega$, a high-Reynolds number flow

APPROVED BY

Timo Siikonen November 15, 2012

Contents

1 Introduction

In a recent study [1] it was shown that some values of the free-stream turbulence caused a friction factor to behave in a peculiar way, when the SST $k-\omega$ turbulence model [2, 3, 4] is used. A similar behavior has taken place in aerodynamic simulations. Usually the SST model works fine, but occasionally either no turbulence is generated or the result is clearly non-physical. This is the case, when the free-stream values are given via input. The default values have worked in a number of simulations made during the past years, but there are different suggestions for them [2, 5].

In a previous study [6] the effect of the free stream values on the SST $k-\omega$ turbulence model was studied by simulating two different cases, a flow over an ogive cylinder and over the Onera M6 wing. Two modifications to the implemented SST $k-\omega$ model were suggested, and the first one was applied. In the present study the same modification is further tested at high Reynolds numbers by simulating a flow over a 200 m long flat plate. Different free stream values are used in two cases, an air flow at a speed of 10 m/s and a water flow at a speed of 5 m/s. Corresponding Reynolds numbers are $1.29 \cdot 10^8$ and $1 \cdot 10^9$.

In a following, the turbulence model is firstly described, then simulation cases and grids are introduced. Finally, the results of the simulations are presented.

2 Flow Equations

A low-Reynolds number approach is used in FINFLO. The Reynolds-averaged Navier-Stokes equations, and the equations for the kinetic energy (k) and specific dissipation (ω) of turbulence can be written in the following form

$$\frac{\partial U}{\partial t} + \frac{\partial (F - F_v)}{\partial x} + \frac{\partial (G - G_v)}{\partial y} + \frac{\partial (H - H_v)}{\partial z} = Q \tag{1}$$

where the unknowns are $U = (\rho, \rho u, \rho v, \rho w, E, \rho k, \rho \omega)^T$. The inviscid fluxes are

$$F = \begin{pmatrix} \rho u \\ \rho u^2 + p + \frac{2}{3}\rho k \\ \rho v u \\ \rho w u \\ (E + p + \frac{2}{3}\rho k)u \\ \rho u k \\ \rho u \omega \end{pmatrix} G = \begin{pmatrix} \rho v \\ \rho u v \\ \rho v^2 + p + \frac{2}{3}\rho k \\ \rho w v \\ (E + p + \frac{2}{3}\rho k)v \\ \rho v k \\ \rho v \omega \end{pmatrix} H = \begin{pmatrix} \rho w \\ \rho u w \\ \rho v w \\ \rho w^2 + p + \frac{2}{3}\rho k \\ (E + p + \frac{2}{3}\rho k)w \\ \rho w k \\ \rho w \omega \end{pmatrix} \tag{2}$$

where ρ is the density, the velocity vector by using Cartesian components is $\vec{V} = u\vec{i} + v\vec{j} + w\vec{k}$, p is the pressure, k is the turbulent kinetic energy and ω its dissipation, and the total energy E is defined as

$$E = \rho e + \frac{\rho \vec{V} \cdot \vec{V}}{2} + \rho k \tag{3}$$

where e is the specific internal energy. The viscous fluxes are

$$F_v = \begin{pmatrix} 0 \\ \tau_{xx} \\ \tau_{xy} \\ \tau_{xz} \\ u\tau_{xx} + v\tau_{xy} + w\tau_{xz} - q_x \\ \mu_k(\partial k/\partial x) \\ \mu_\omega(\partial \omega/\partial x) \end{pmatrix} G_v = \begin{pmatrix} 0 \\ \tau_{xy} \\ \tau_{yy} \\ \tau_{yz} \\ u\tau_{xy} + v\tau_{yy} + w\tau_{yz} - q_y \\ \mu_k(\partial k/\partial y) \\ \mu_\omega(\partial \omega/\partial y) \end{pmatrix}$$

$$H_v = \begin{pmatrix} 0 \\ \tau_{xz} \\ \tau_{yz} \\ \tau_{zz} \\ u\tau_{xz} + v\tau_{yz} + w\tau_{zz} - q_z \\ \mu_k(\partial k/\partial z) \\ \mu_\omega(\partial \omega/\partial z) \end{pmatrix} \tag{4}$$

Here the stress tensor, τ_{ij}, includes laminar and turbulent components. The fluid is assumed to be Newtonian and, therefore, the laminar stresses are modelled by using Stokes hypothesis. The Reynolds stresses $\overline{\rho u_i'' u_j''}$ are included in the stress tensor τ_{ij}.

$$\tau_{ij} = \mu \left[\frac{\partial u_j}{\partial x_i} + \frac{\partial u_i}{\partial x_j} - \frac{2}{3}(\nabla \cdot \vec{V})\delta_{ij} \right] - \overline{\rho u_i'' u_j''} + \frac{2}{3}\rho k \delta_{ij} \tag{5}$$

For the Reynolds stresses, Boussinesq's approximation

$$-\overline{\rho u_i'' u_j''} = \mu_T \left[\frac{\partial u_j}{\partial x_i} + \frac{\partial u_i}{\partial x_j} - \frac{2}{3}(\nabla \cdot \vec{V})\delta_{ij} \right] - \frac{2}{3}\rho k \delta_{ij} \tag{6}$$

is utilized in RANS simulations. Here μ_T is a turbulent viscosity coefficient, which is calculated by using a turbulence model, and δ_{ij} is the Kronecker's delta. In the momentum and energy equations, the kinetic energy contribution $2/3\rho k \delta_{ij}$ has been connected with pressure and appears in the convective fluxes, whereas the diffusive part is connected with the viscous fluxes. The viscous stresses contains a laminar and a turbulent parts. The heat flux can be written as

$$\vec{q} = -(\lambda + \lambda_T)\nabla T = -\left(\mu \frac{c_p}{Pr} + \mu_T \frac{c_p}{Pr_T} \right) \nabla T \tag{7}$$

where λ is a molecular and λ_T a turbulent thermal conductivity coefficient and Pr is a laminar and Pr_T a turbulent Prandtl number, and c_p is a specific heat at constant pressure. The diffusion of turbulence variables is modelled as

$$\mu_k \nabla k = \left(\mu + \frac{\mu_T}{\sigma_k}\right) \nabla k \tag{8}$$

$$\mu_\omega \nabla \omega = \left(\mu + \frac{\mu_T}{\sigma_\omega}\right) \nabla \omega \tag{9}$$

where σ_k and σ_ω are turbulent Schmidt numbers of k and ω, respectively. Density is obtained from an equation of state $\rho = \rho(p, T)$ Since the case for the ogive cylinder is incompressible, pressure differences $p - p_0$ are solved instead of pressure. The components of the source term Q are non-zero in possible buoyancy terms and in turbulence model equations.

In the present study both preconditioning and pressure correction methods are used to determine the pressure. The solution method applied is presented in [7], and the pressure correction method used is described in [8]. As compared to the traditional pressure correction methods, the basic difference of the present method is that all the residuals are calculated simultaneously and only once during an iteration cycle. The complexity of the coupled implicit solution is avoided by manipulating the explicit residuals. Since the same explicit stage is used as in preconditioning, the pressure correction can be used as a parallel solution method for the preconditioning.

3 SST $k - \omega$ RANS-model

3.1 Basic Model

The model equations using an implicit summation over j-index are

$$\begin{aligned} \rho\frac{\partial k}{\partial t} + \rho u_j \frac{\partial k}{\partial x_j} &= P - \beta^* \rho k \omega \\ &+ \frac{\partial}{\partial x_j}\left[(\mu + \frac{\mu_T}{\sigma_k})\frac{\partial k}{\partial x_j}\right] \end{aligned} \tag{10}$$

$$\begin{aligned} \rho\frac{\partial \omega}{\partial t} + \rho u_j \frac{\partial \omega}{\partial x_j} &= \frac{\gamma\rho}{\mu_T} P - \beta\rho\omega^2 \\ &+ \frac{\partial}{\partial x_j}\left[(\mu + \frac{\mu_T}{\sigma_\omega})\frac{\partial \omega}{\partial x_j}\right] \\ &+ 2\rho\frac{1 - F_1}{\sigma_{\omega 2}\omega}\frac{\partial k}{\partial x_j}\frac{\partial \omega}{\partial x_j} \end{aligned} \tag{11}$$

The model coefficients in Eqs. (10) and (11) are obtained from

$$(\sigma_k \ \sigma_\omega \ \beta)^T = F_1 \, (\sigma_k \ \sigma_\omega \ \beta)_1^T + (1 - F_1) \, (\sigma_k \ \sigma_\omega \ \beta)_2^T \tag{12}$$

with the following values

$$\begin{array}{lll} \sigma_{k1} = 1.176 & \sigma_{\omega 1} = 2.0 & \beta_1 = 0.075 \\ \sigma_{k2} = 1.0 & \sigma_{\omega 2} = 1.168 & \beta_2 = 0.0828 \end{array}$$

Coefficients κ and β^* have constant values of 0.41 and 0.09. Coefficient γ is calculated from

$$\gamma = \frac{\beta}{\beta^*} - \frac{\kappa^2}{\sigma_\omega \sqrt{\beta^*}} \tag{13}$$

Term P in Eqs. (10) and (11) is the production of turbulent kinetic energy and calculated using the Boussinesq approximation from Eq. (6). The last term in the ω-equation originates from the transformed ϵ-equation and it is called a cross-diffusion term. The switching function which governs the choice between the ω- and the ϵ-equations is

$$F_1 = \tanh\left(\Gamma^4\right) \tag{14}$$

where

$$\Gamma = \min\left(\max\left(\frac{\sqrt{k}}{\beta^*\omega d}; \frac{500\nu}{\omega d^2}\right); \frac{4\rho\sigma_{\omega 2}k}{CD_{k\omega}d^2}\right) \tag{15}$$

The first term is a turbulent length scale divided with the distance from the walls (d). This ratio is around 2.5 in a logarithmic layer and approaches zero in an outer layer. The second term has a value of ≥ 1 only in a viscous sublayer. The meaning of the third term is to ensure stable behaviour of F_1 when the value of ω in the free stream is small. It utilizes a parameter

$$CD_{k\omega} = \max\left(\frac{2\rho}{\sigma_{\omega 2}\omega}\frac{\partial k}{\partial x_j}\frac{\partial \omega}{\partial x_j}; CD_{k\omega\,\min}\right) \tag{16}$$

which is a lower limit of the cross diffusion term. The main purpose of the switching function is to limit the use of the $k-\omega$ model into the boundary layer region. The switch may be a weak point in the model, but it seems to work at least in cases of external flows.

Free-stream boundary conditions are also applied as lower limits for k and ω in FINFLO. These limits, especially too high a value for ω_∞, may lead to troubles on the outer edege of the boundary layer. The original suggestions are [2]:

$$\begin{aligned} \frac{u_\infty}{L_{\text{ref}}} < \omega_\infty < 10\frac{u_\infty}{L_{\text{ref}}} \\ \frac{10^{-5}u_\infty^2}{Re_{L_{\text{ref}}}} < k_\infty < \frac{0.1u_\infty^2}{Re_{L_{\text{ref}}}} \end{aligned} \tag{17}$$

In FINFLO the lower limit has been chosen for ω_∞, whereas the multiplier in the second condition is 10^{-3}. This indicates that $u_{T\infty}/\mu_\infty = 10^{-3}$ and $k_\infty = u_\infty^2/Re_{L_{\text{ref}}}$. Thus at high Reynolds numbers the turbulence level approaches zero and ω_∞ also has a low value, while the eddy viscosity remains constant.

Another variant for the free stream values has been given by Spalart and Rumsey [5]:

$$\begin{aligned} \omega_\infty &= \frac{5u_\infty}{L_{\text{ref}}} \\ k &= 10^{-6}u_\infty^2 \end{aligned} \tag{18}$$

The corresponding eddy viscosity is $\mu_{T\infty}/\mu_\infty = 10^{-6}Re_{L_{\text{ref}}}/5$. At a high Reynolds number this results in a huge eddy viscosity, whereas the turbulence level is reasonably low.

3.2 Modifications

On the basis of the sample calculations it was decided to change the relationships between the turbulence quantities. A goal was that the free-stream conditions could be given more freely. As a first trial the turbulence production terms are changed. In the simulations where unphysical solutions have been obtained, the free-stream value of ω has been large. A simple and well known trick to remove the effect of free-stream ω_∞ is to add a corresponding production on the right hand side of Eq. (10)

$$\beta^*\rho_\infty k_\infty \omega_\infty$$

This is called a SST-sust model [5]. As a result the free-stream turbulence never dies out as is the case without this term. In practice the evident decay is prevented by specifying a lower limit, i.e. the 'free-stream' value for the kinetic energy of turbulence. (In spite of the correction term this limitation is applied in order to ensure a realizability of the model).

For the ω-equation a corresponding term is needed on the right-hand side of Eq. (11)

$$\beta\rho_\infty\omega_\infty^2$$

With these corrections k and ω behave realistically in the free stream and the possibly large value of ω_∞ does not disturb the outer boundary layer. However, the turbulent viscosity remains unaffected and has a value specified via input. It is also possible to modify the equation for the eddy viscosity. In the SST model this is calculated from

$$\mu_T = \frac{a_1\rho k}{\max\left(a_1\omega, SF_2\right)} \tag{19}$$

where $a_1 = 0.31$ is Bradshaw's constant, $S = \sqrt{2S_{ij}S_{ij}}$ is the absolute value of a strain rate tensor

$$S_{ij} = \frac{1}{2}\left(\frac{\partial u_i}{\partial x_j} + \frac{\partial u_j}{\partial x_i}\right) \tag{20}$$

and function F_2 is calculated from

$$F_2 = \tanh\left(\Gamma_2^2\right) \tag{21}$$

where

$$\Gamma_2 = \max\left(\frac{2\sqrt{k}}{\beta^*\omega d}; \frac{500\nu}{\omega d^2}\right) \tag{22}$$

A second method for removing the effect of a large background value of ω can be based on a modification of the viscosity formula. For a free stream a suitable value for a maximum ω_∞ can be found on the basis of validation calculations. Since function F_2 is small outside the boundary layer, the eddy viscosity can be approximated as

$$\mu_{T,\infty} = \frac{\rho_\infty k_\infty}{\omega_0 + \omega_\infty} \tag{23}$$

Since k_∞ and $\mu_{T,\infty}$ are given via input and the lower limit for ω_∞ has the specified default value, parameter ω_0 can be solved. This parameter is applied throughout the computational domain, but only in connection with Eq. (19) and its influence is small in viscous regions. Thus a combination of $\mu_{T,\infty}$ and k_∞ does not lead to a large value of ω_∞, which seems to be the main cause of troubles with the SST-model.

4 Computational Domain and Grid

The modifications are tested with a simple flat-plate geometry at two high Reynolds numbers. The flat plate is 200 m long and the height of the grid is 5 m. The first cell height is $1.5 \cdot 10^{-4}$ m. After that the ratio between the neighboring cells is $\Delta y_{n+1}/\Delta y_n = 1.1$ in a wall normal direction, $\Delta y_{n+1}/\Delta y_n = 1.08$ for the first 50 m in a streamwise direction and $\Delta y_{n+1}/\Delta y_n \approx 1.00$ after that. The resulting grid size is 160×96.

A uniform velocity distribution is given as an inlet condition. The pressure is extrapolated from the computational domain. At the lower boundary symmetry conditions are applied before the flat plate. At the flat plate the velocities and the kinetic energy of the turbulence are set to zero. Pressure is given and zero gradients are assumed at the outlet and on the boundary parallel to the plate. Temperature is constant along the plate.

5 Results

Two cases are simulated, one using air as a fluid and another using water. Free stream velocity is 10 m/s with air and 5 m/s with water. Reynolds numbers are $Re = 1.3 \cdot 10^8$ and $Re = 10^9$, respectively. The simulations were started on the third grid level and the result was interpolated on the finer levels until the first level was reached. Two multigrid levels are used to accelerate convergence. A third-order upwind biased discretization is used in the calculation of the convective fluxes. A Courant number is $CFL = 3$ in all cases.

5.1 Air ($Re = 1.3 \cdot 10^8$)

Four different sets of free stream turbulence values are utilized in simulations. In 'Case 1' values suggested in Ref. [5], $k_\infty = 1{\cdot}10^{-6}U_\infty^2$ and $\omega_\infty = 5U_\infty/L_{\text{ref}}$ are applied. These yield to a turbulence intensity and turbulent viscosity values of $Tu = 0.0008165$ and $\mu_T/\mu = 26.1437$, respectively. In 'Case 2' and 'Case 3' these values are $Tu = 0.001$ and $\mu_T/\mu = 0.01$. In 'Case 4' the default values computed by the solver are applied resulting in of $Tu = 2.25568 \cdot 10^{-6}$ and $\mu_T/\mu = 0.001$. In Case 2 the first modification described is used and in Case 3 the original model is applied. Free stream values for turbulence is presented in Table 1.

Table. 1: Free stream values.

	k_∞	ω_∞	μ_T/μ	Tu
Case 1	0.0001	0.2976970	26.1437	0.0008165
Case 2	0.00015	1167.425	0.01	0.001
Case 3	0.00015	1167.425	0.01	0.001
Case 4	$7.6318 \cdot 10^{-10}$	0.0594	0.001	$2.25568 \cdot 10^{-6}$

5.1.1 Convergence

The convergence histories for the Case 1 and Case 2 are shown in Figs. 1 - 4. The density residual is converged within 100 cycles, but the momentum residual in x-direction needs nearly 3 000 cycles and over 5 000 cycles with modification 1. The budgets of turbulent kinetic energy are on a totally different level between the cases as well as the budgets of dissipation of the turbulent kinetic energy.

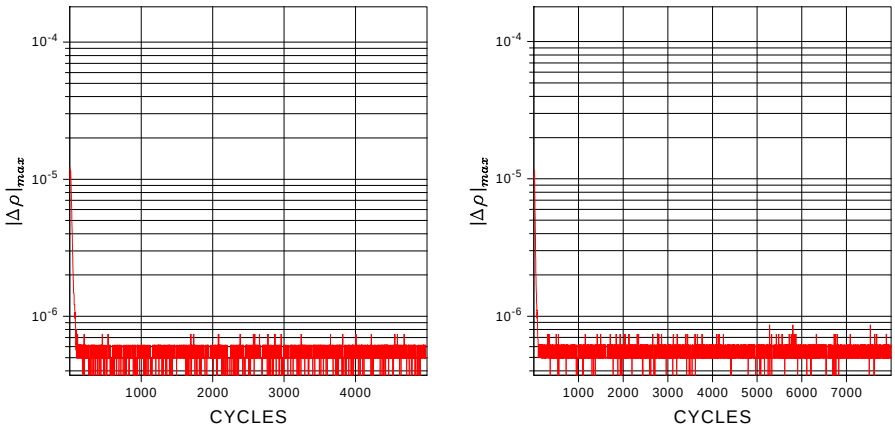

Fig. 1: Convergence history of $||\Delta\rho||_2$. Case 1 on the left and Case 2 on the right.

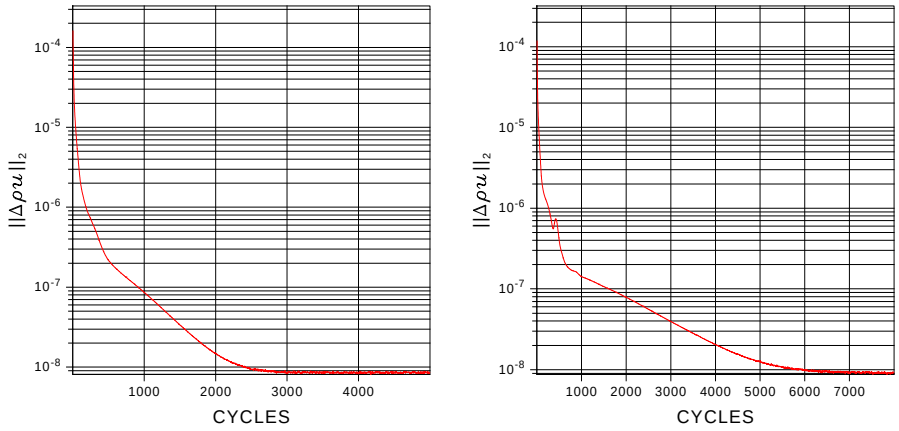

Fig. 2: Convergence history of $||\Delta\rho u||_2$. Case 1 on the left and Case 2 on the right.

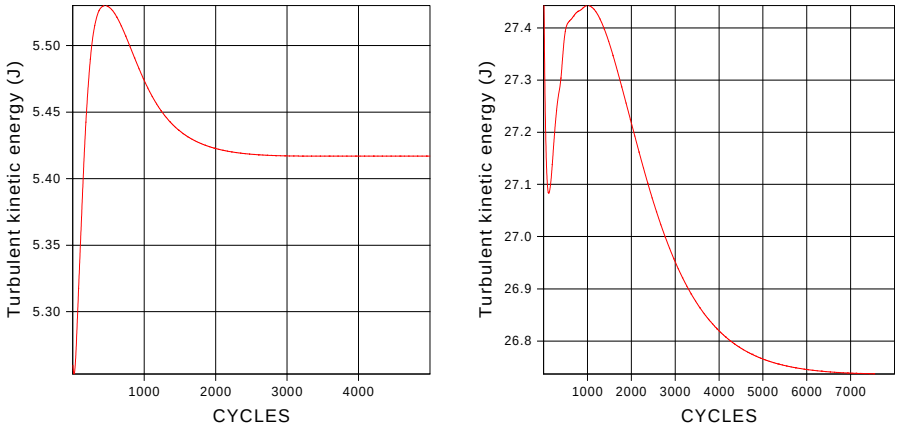

Fig. 3: Convergence history of the budget of the kinetic energy of turbulence. Case 1 on the left and Case 2 on the right.

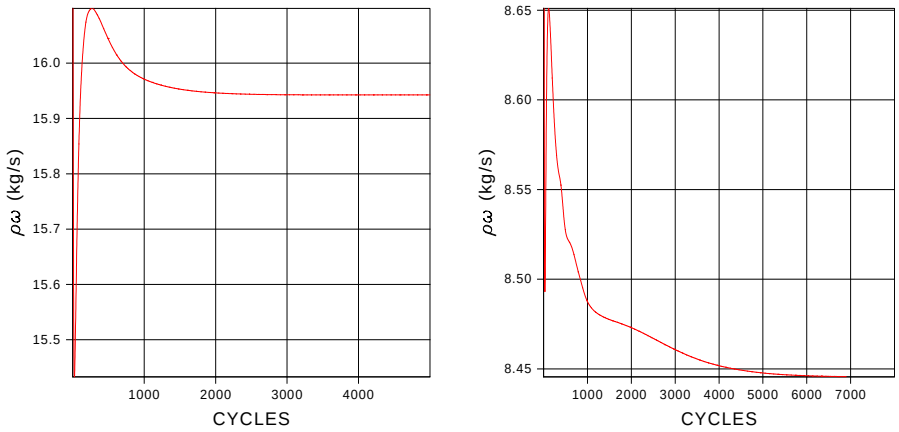

Fig. 4: Convergence history the budget of dissipation of turbulent kinetic energy. Case 1 on the left and Case 2 on the right.

5.1.2 Free Stream and Boundary Layer

Universal boundary layer parameters, friction factor C_f, pressure coefficient C_p, boundary layer thickness δ_{99} defined as a height where the velocity is 99 % of the free stream velocity, displacement thickness δ^*_{99}, momentum thickness θ and shape factor H, are shown in Figs. 5 - 7. The displacement thickness, the momentum thickness and the shape function are defined as

$$\delta^*_{99} = \int_0^{\delta_{99}} \left(1 - \frac{u(y)}{U_e}\right) dy \tag{24}$$

$$\theta = \int_0^{\delta_{99}} \frac{u(y)}{U_e} \left(1 - \frac{u(y)}{U_e}\right) dy \tag{25}$$

$$H = \frac{\delta^*_{99}}{\theta} \tag{26}$$

where $U_e \equiv u_\infty$ is the velocity at the edge of the boundary layer.

There are significant differences between cases, so that in Cases 1 and 4 the values are similar and Cases 2 and 3 differ from those. Usually Case 2 is closer to Cases 1 and 4 than Case 3, which is calculated without the modification. An exception is pressure coefficient, where Case 2 is oscillating after the location $Re_x = 4 \cdot 10^7$.

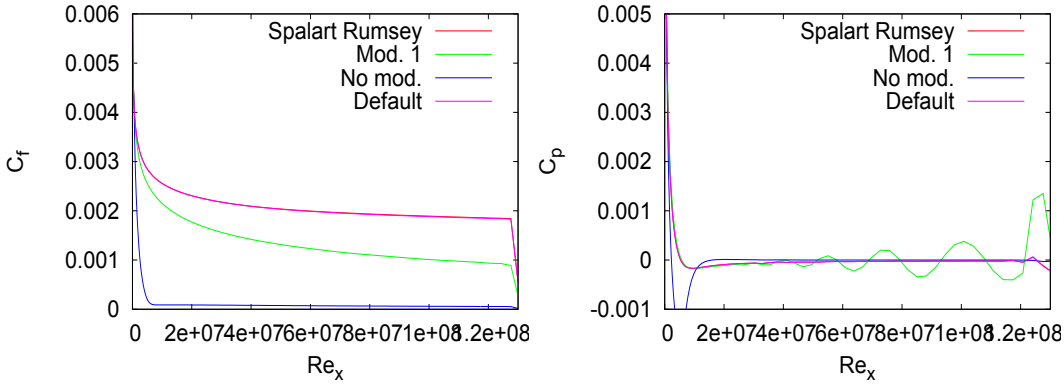

Fig. 5: Friction coefficient (left) and pressure coefficient(right along the plate.)

Velocity profiles in a half-logarithmic scale are shown in Figs. 8 and 9. Again, Cases 1 and 4 are quite similar but there is a small difference between those and Cases 2 and 3 already at $Re_x = 6.5 \cdot 10^5$. The difference is growing larger into the downstream direction of the plate.

Profiles of the turbulent kinetic energy are shown in Figs. 10 and 11 and dimensionless turbulent viscosity in Figs. 12 and 13, both in a logarithmic scale. Turbulent kinetic energy of Case 2 differs a lot from the others in the boundary layer, while Case 3 turns to a laminar solution. Turbulent viscosity profiles are quite similar for Cases 1 and 4 in the boundary layer, Case 1 is clearly different in the free stream region.

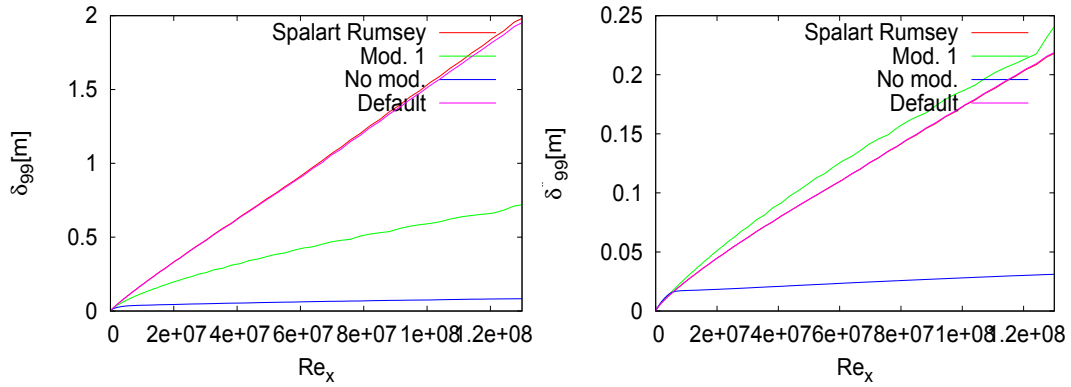

Fig. 6: Boundary layer thickness (left) and displacement thickness (right) along the plate.

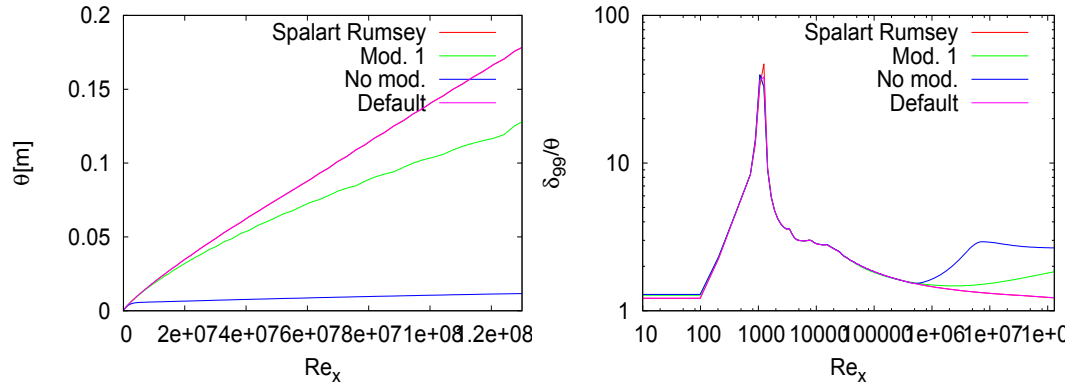

Fig. 7: Momentum thickness (left) and shape factor (right) along the plate.

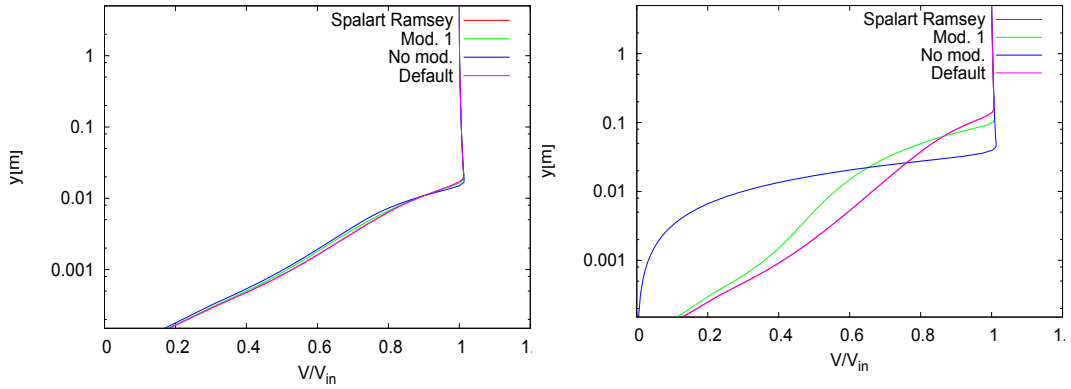

Fig. 8: Velocity distributions at locations $Re_x = 6.5 \cdot 10^5$ and $Re_x = 6.5 \cdot 10^6$.

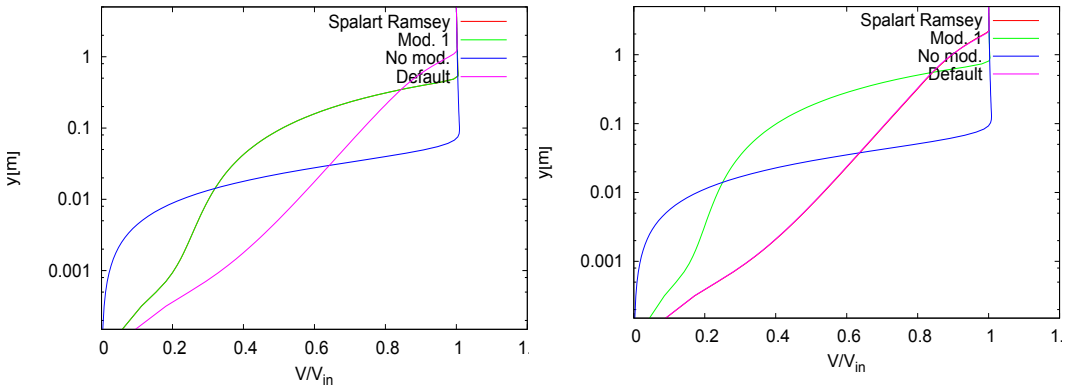

Fig. 9: Velocity distributions at locations $Re_x = 6.5 \cdot 10^7$ and $Re_x = 1.3 \cdot 10^8$.

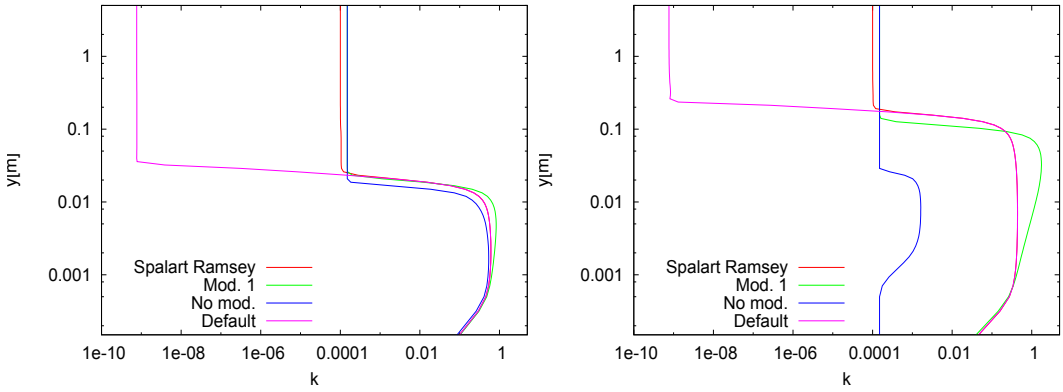

Fig. 10: Distributions of the turbulent kinetic energy at locations $Re_x = 6.5 \cdot 10^5$ and $Re_x = 6.5 \cdot 10^6$.

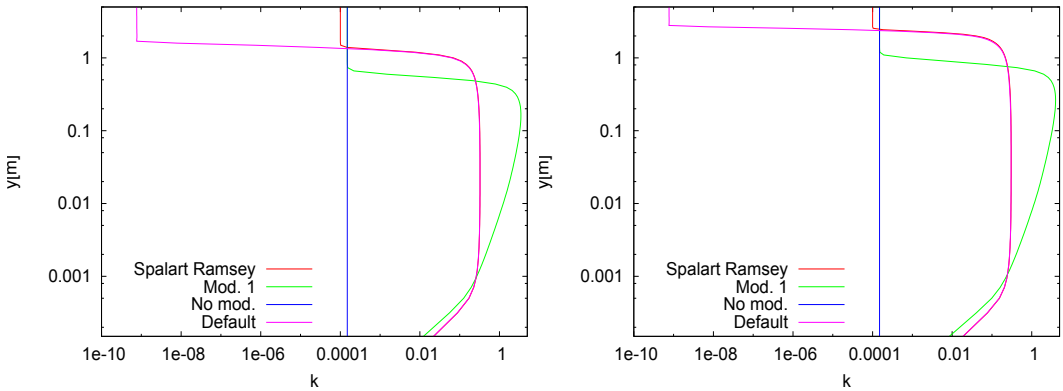

Fig. 11: Distributions of the turbulent kinetic energy at locations $Re_x = 6.5 \cdot 10^7$ and $Re_x = 1.3 \cdot 10^8$.

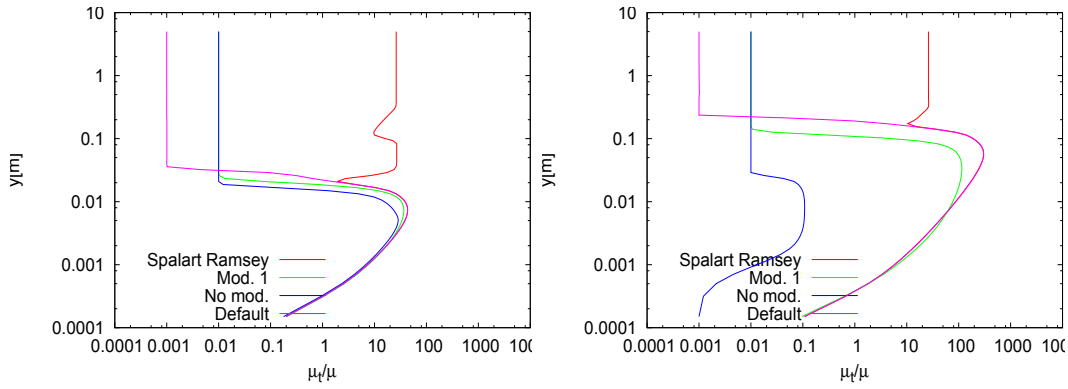

Fig. 12: Distributions the turbulent viscosity at locations $Re_x = 6.5 \cdot 10^5$ and $Re_x = 6.5 \cdot 10^6$.

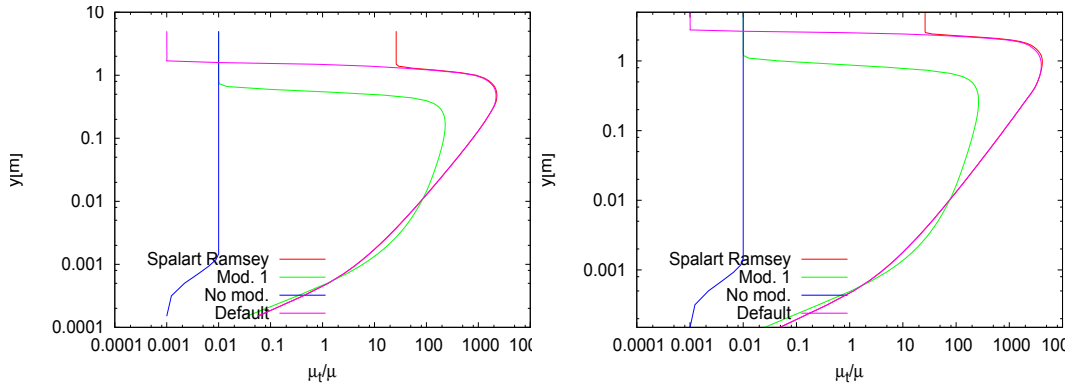

Fig. 13: Distributions the turbulent viscosity at locations $Re_x = 6.5 \cdot 10^7$ and $Re_x = 1.3 \cdot 10^8$.

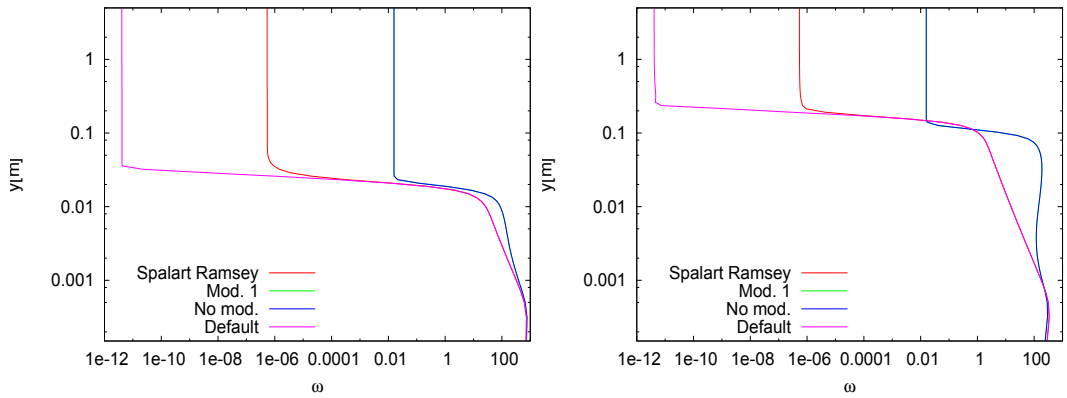

Fig. 14: Distributions of specific dissipation rate ω at locations $Re_x = 6.5 \cdot 10^5$ and $Re_x = 6.5 \cdot 10^6$.

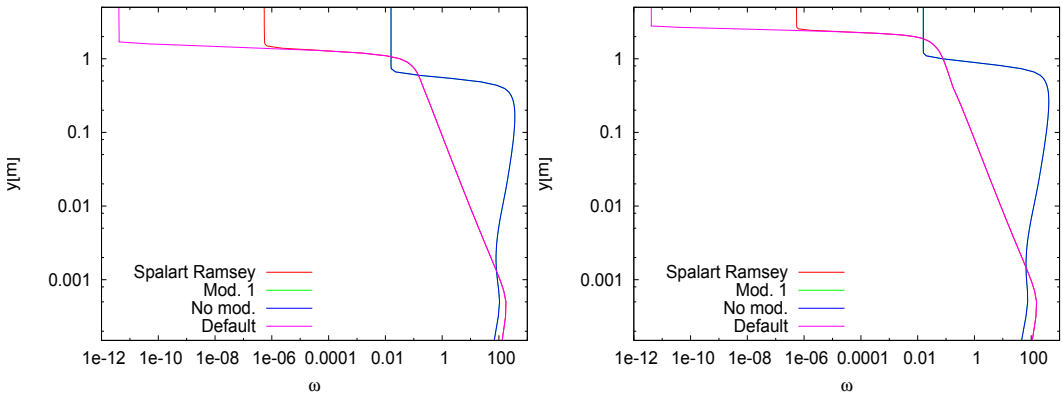

Fig. 15: Distributions of specific dissipation rate ω at locations $Re_x = 6.5 \cdot 10^7$ and $Re_x = 1.3 \cdot 10^8$.

5.2 Water ($Re = 1 \cdot 10^9$)

With water a very high Reynolds number is obtained. As in simulations with air, four different sets of the free stream turbulence values are utilized in simulations. In 'Case 1' values suggested in Ref. [5], $k_\infty = 1 \cdot 10^{-6} U_\infty^2$ and $\omega_\infty = 5U_\infty / L_{\text{ref}}$ are applied. These yield to a turbulence intensity and turbulent viscosity values of $Tu = 0.0008165$ and $\mu_T/\mu = 208.55$, respectively. In 'Case 2' and 'Case 3' these values are $Tu = 0.001$ and $\mu_T/\mu = 0.1$. In 'Case 4' these values are computed by the solver resulting values $Tu = 4.086 \cdot 10^{-7}$ and $\mu_T/\mu = 0.001$. As in the simulation with air, in Case 2 the modification described (Eq. 19) is applied. Free stream values for turbulence are presented in Table 2.

Table. 2: Free stream values.

	k_∞	ω_∞	μ_T/μ	Tu
Case 1	0.000025	119.67	208.55	0.0008165
Case 2	0.0000375	1167.425	0.1	0.001
Case 3	0.0000375	374345.4	0.1	0.001
Case 4	$2.504 \cdot 10^{-11}$	25.0	0.001	$4.086 \cdot 10^{-7}$

5.2.1 Convergence

The convergence histories for the Case 1 and Case 2 are shown in Figs. 16 - 19. The convergence in these cases is comparable to corresponding simulations with air, although the convergence is now a bit slower as a consequence of the higher Reynolds number.

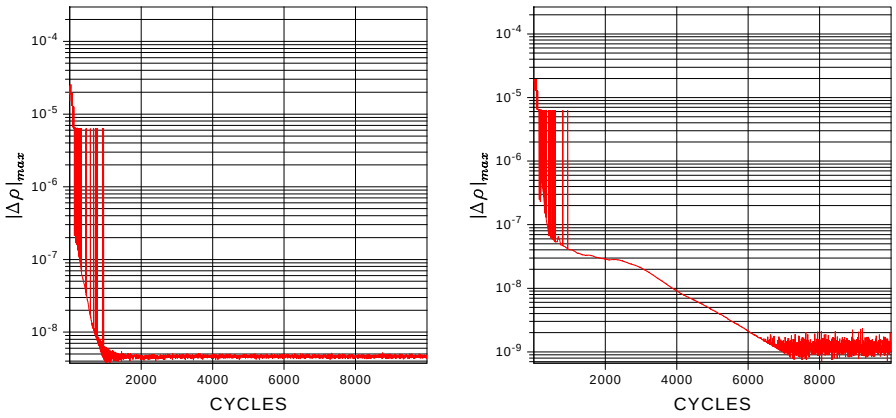

Fig. 16: Convergence history of $||\Delta\rho||_2$. Case 1 on the left and Case 2 on the right.

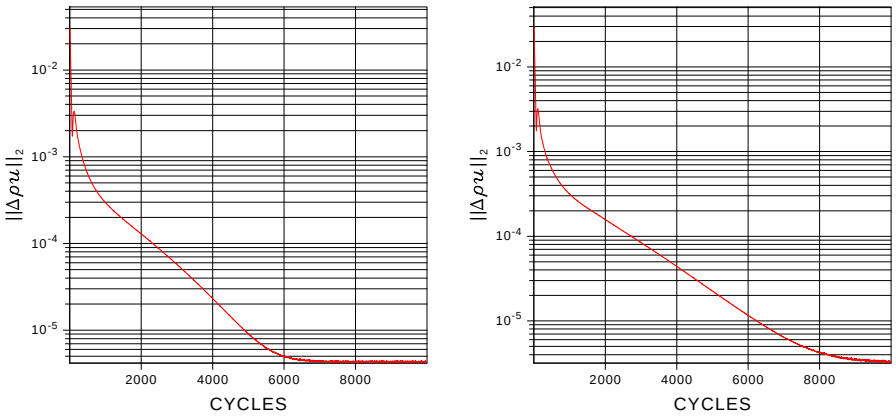

Fig. 17: Convergence history of $||\Delta\rho u||_2$. Case 1 on the left and Case 2 on the right.

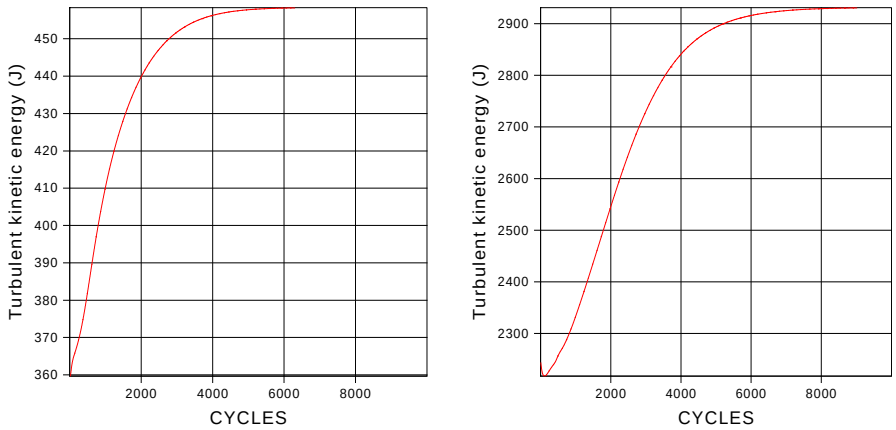

Fig. 18: Convergence history of the budget of the kinetic energy of turbulence. Case 1 on the left and Case 2 on the right.

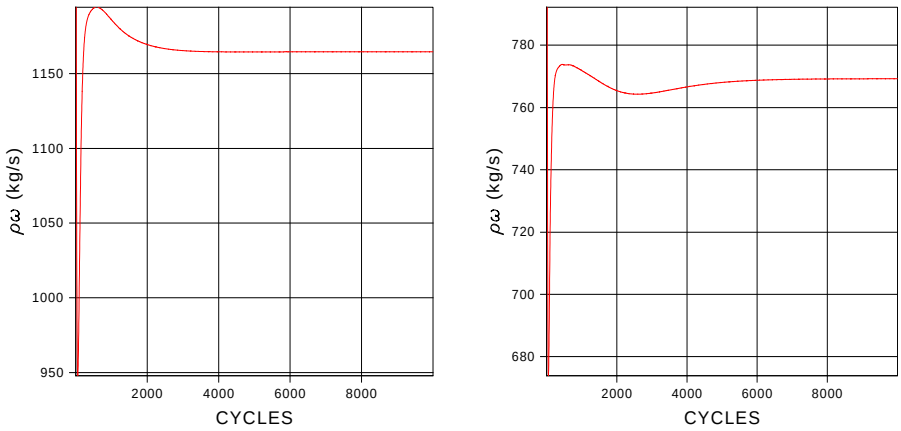

Fig. 19: Convergence history the budget of dissipation of turbulent kinetic energy. Case 1 on the left and Case 2 on the right.

5.2.2 Free Stream and Boundary Layer

The boundary layer parameters, friction factor C_f, pressure coefficient C_p, boundary layer thickness δ_{99}, displacement thickness δ^*_{99}, momentum thickness θ and shape factor H, are shown in Figs. 20 - 22. Again there are significant differences between cases, so that in Cases 1 and 4 the values are similar and Cases 2 and 3 differ from those. There is also significant difference between Cases 2 and 3.

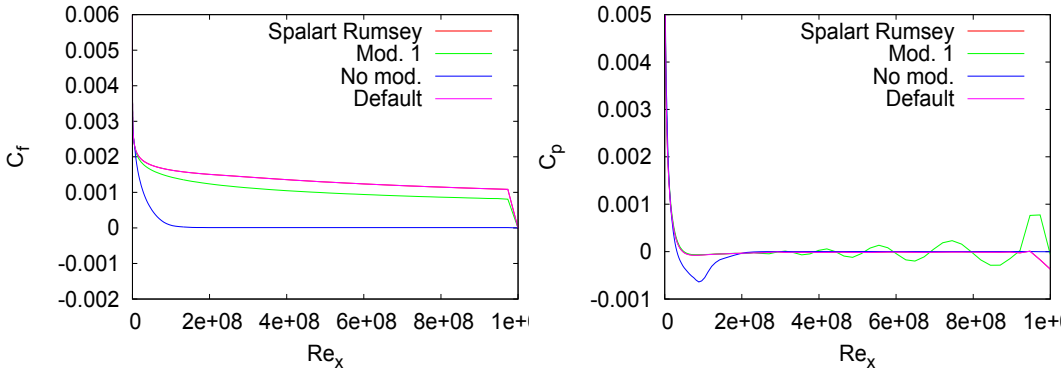

Fig. 20: Friction coefficient (left) and pressure coefficient(right along the plate.)

Velocity profiles in a half-logarithmic scale are shown in Figs. 23 and 24. The velocity distributions are well aligned at a distance of 1 m ($Re_x = 5 \cdot 10^5$) after the entrance, but as with air differences are growing larger downstream the plate.

Profiles of the turbulent kinetic energy are shown in Figs. 25 and 26 and dimensionless turbulent viscosity in Figs. 27 and 28, both in a logarithmic scale.

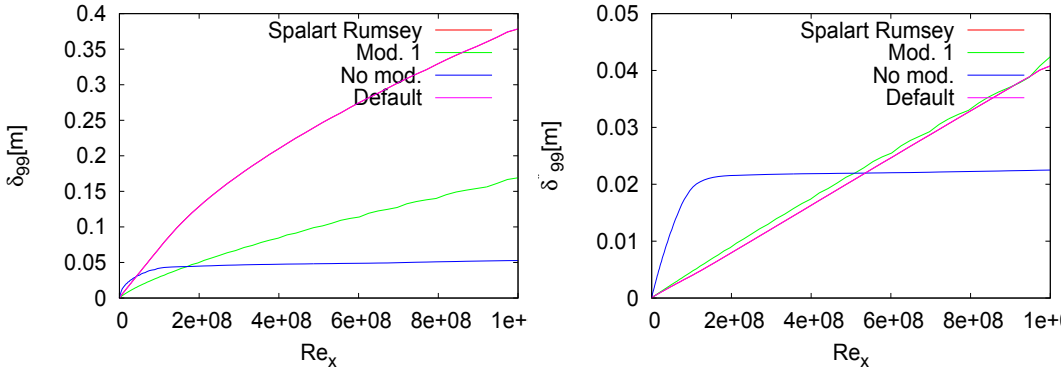

Fig. 21: Boundary layer thickness (left) and displacement thickness (right) along the plate.

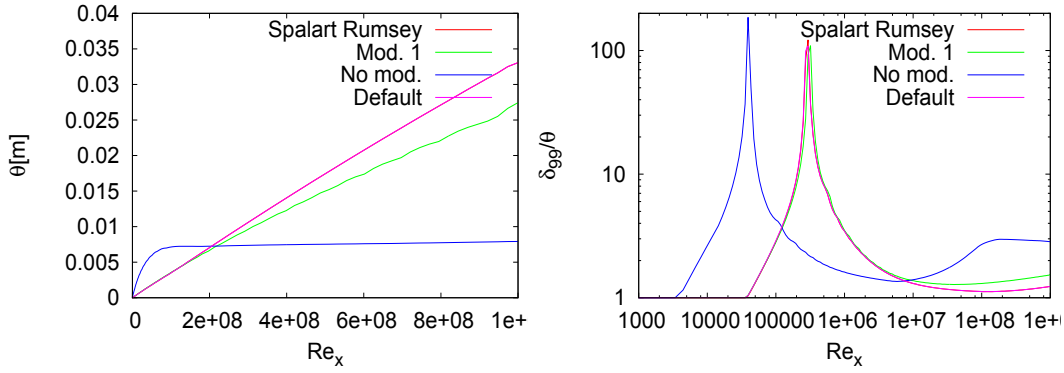

Fig. 22: Momentum thickness (left) and shape factor (right) along the plate.

Turbulent kinetic energy of Case 3 differs a lot from the others in the boundary layer, since Case 3, i.e. the model with no modifications, turns out to be almost laminar. In a free stream area Cases 1 and 2 are similar. Turbulent viscosity profiles are quite similar for Cases 1 and 4 in the boundary layer, again Case 1 is clearly different in the free stream area.

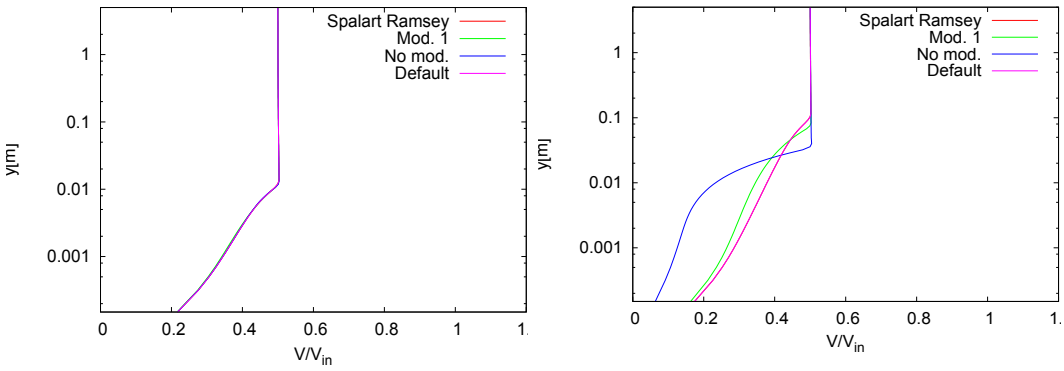

Fig. 23: Velocity distributions at locations $Re_x = 5 \cdot 10^6$ and $Re_x = 5 \cdot 10^7$.

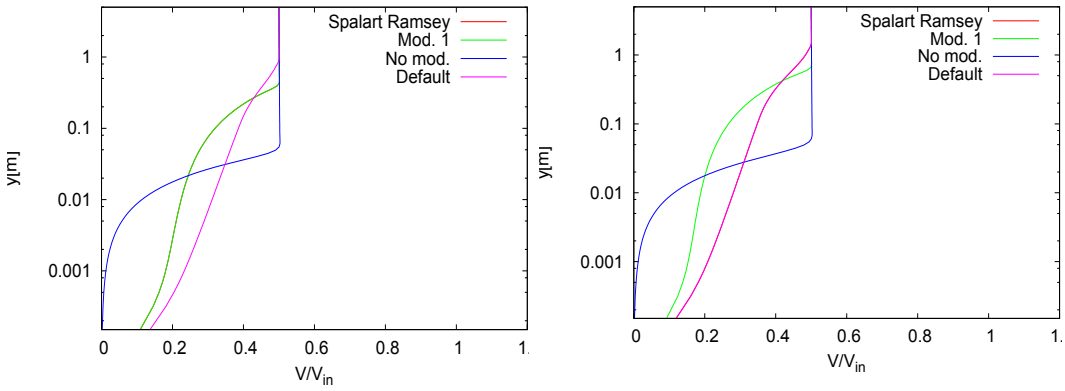

Fig. 24: Velocity distributions at locations $Re_x = 5 \cdot 10^8$ and $Re_x = 10^9$.

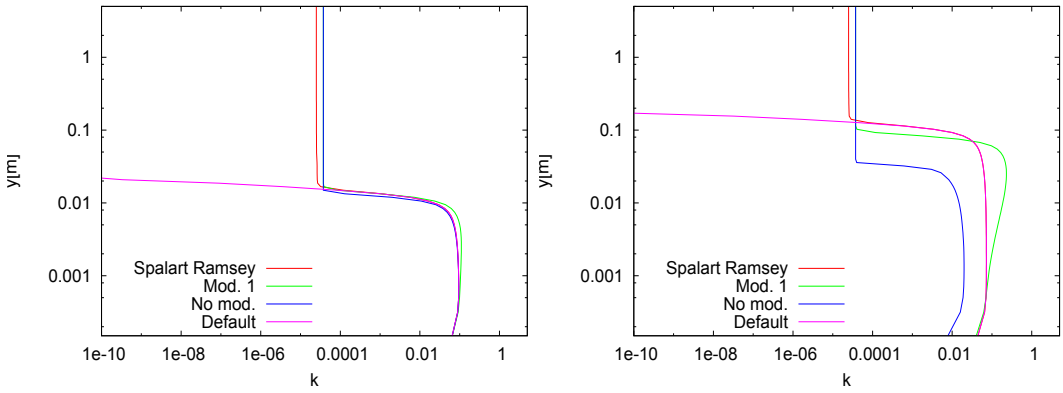

Fig. 25: Distributions of the turbulent kinetic energy at locations $Re_x = 5 \cdot 10^6$ and $Re_x = 5 \cdot 10^7$.

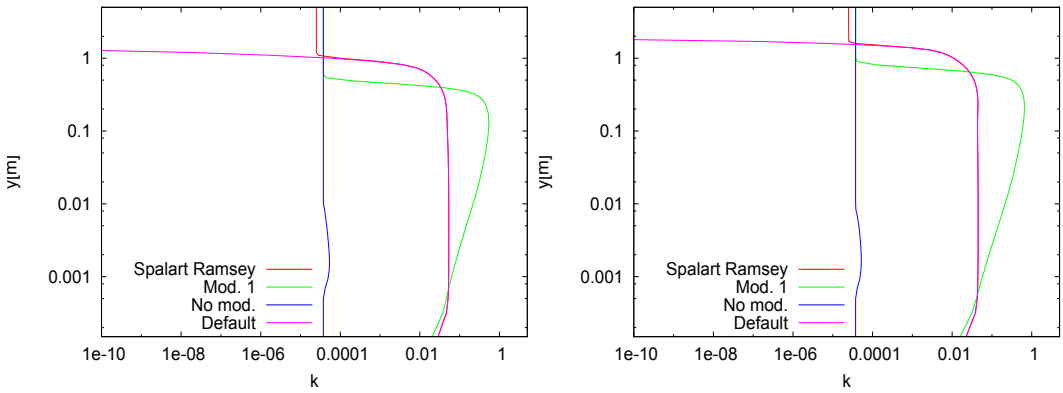

Fig. 26: Distributions of the turbulent kinetic energy at locations $Re_x = 5 \cdot 10^8$ and $Re_x = 10^9$.

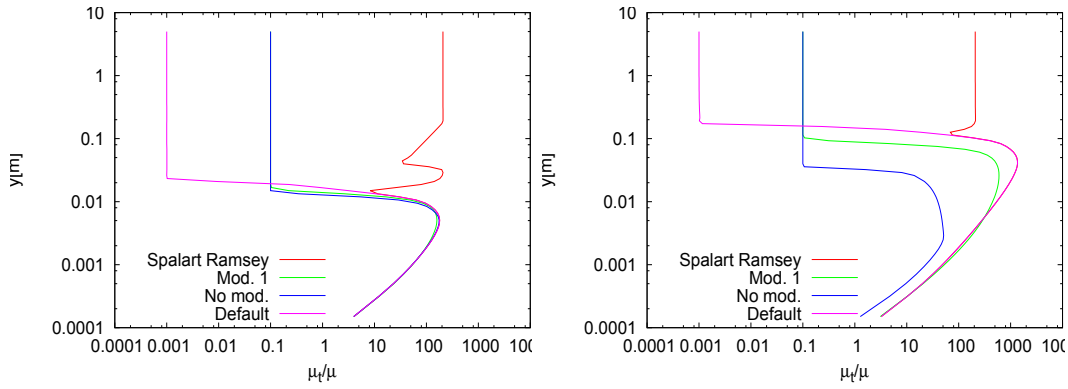

Fig. 27: Distributions the turbulent viscosity at locations $Re_x = 5 \cdot 10^6$ and $Re_x = 5 \cdot 10^7$.

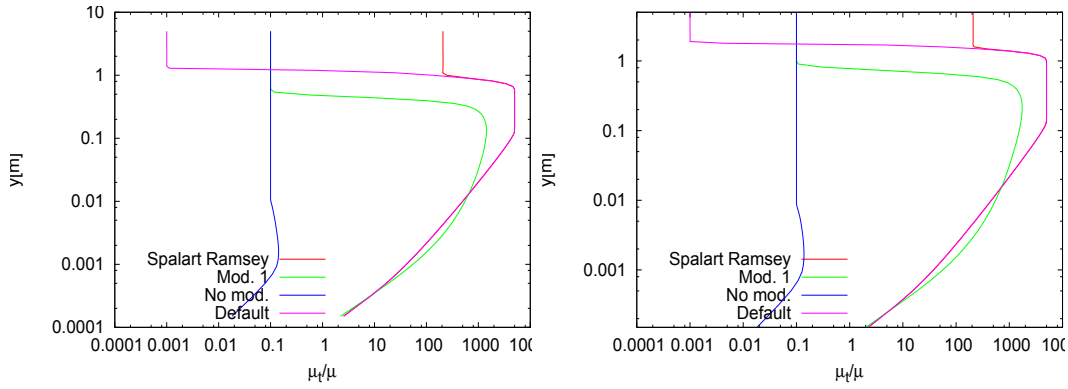

Fig. 28: Distributions the turbulent viscosity at locations $Re_x = 5 \cdot 10^8$ and $Re_x = 10^9$.

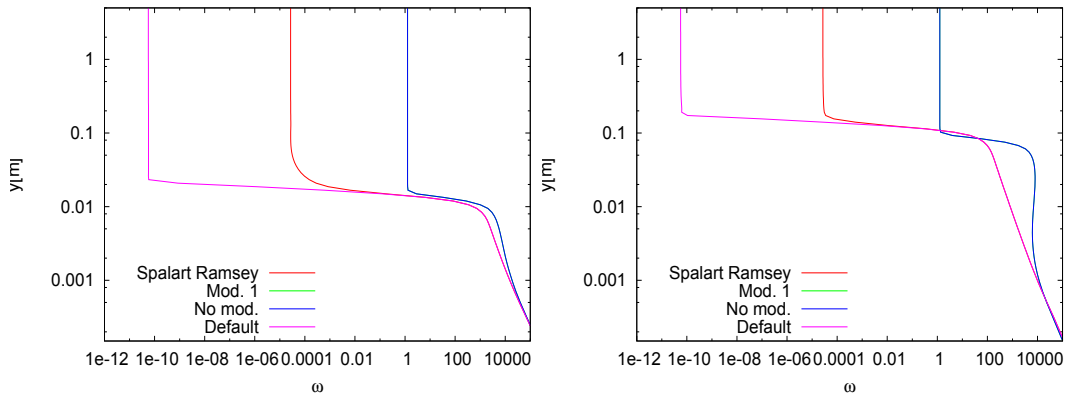

Fig. 29: Distributions of specific dissipation rate ω at locations $Re_x = 5 \cdot 10^6$ and $Re_x = 5 \cdot 10^7$.

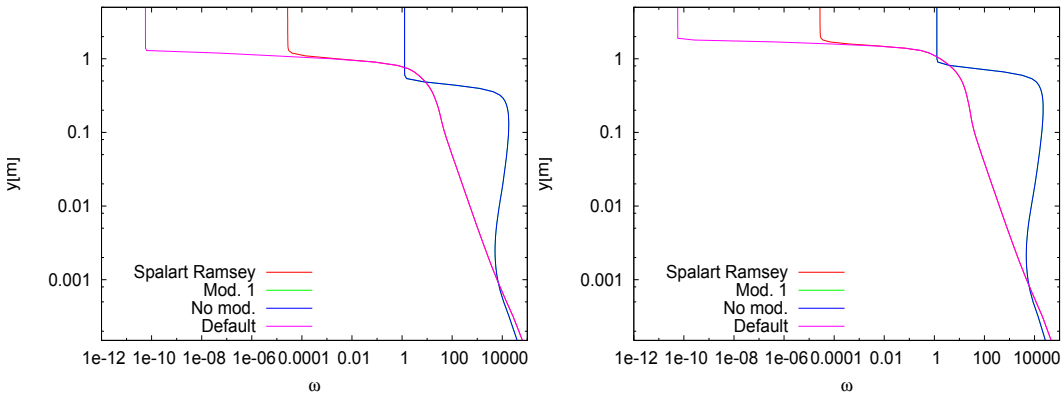

Fig. 30: Distributions of specific dissipation rate ω at locations $Re_x = 5 \cdot 10^8$ and $Re_x = 10^9$.

6 Conclusions

In some simulations it has been found out that the free-stream values for the turbulence quantities may significantly effect the flow solution, as the SST $k - \omega$ model is applied. The original default values usually work well, but the turbulence intensity may have unphysically low a value. The values suggested by Spalart and Rumsey also give sensible results, but result in a high value for the eddy viscosity in a free stream.

Two modifications have been suggested in order to cure the problem and the first one has been tested at high Reynolds numbers. Although the SST-sust model seemed to improve the situation in cases like an ogive cylinder and Onera M6 wing, the present study shows that some values still cause problems in simulations of a high-Reynolds-number flow over a flat plate. There is some improvement in the results as Re_x is sufficiently low, but as Re_x is increased finally the friction factor drops and the velocity profile becomes unphysical. It should be noted that this concerns situations, where the free-stream values are not given according to the recommendations.

In a boundary layer both the values suggested by Spalart and Rumsey and the default values give very similar results provided that the recommended free-stream values are applied. However, in the free-stream the eddy viscosity differs a lot. The default values of the code, i.e. the original ones seem to give the best results in all situations. However, the turbulence intesity that is applied e.g. transition modeling [9, 10] should be specified case by case, not according to the applied default values. This leaves the question about the free-stream values still open.

References

[1] Sipilä, T., "The Effect of Free-Stream Turbulence Parameters on a Flow over an Ogive Cylinder. Research Report VTT-R-08130-11.," VTT Technical Research Centre of Finland, Espoo, 2012.

[2] Menter, F., "Zonal Two Equation $k-\omega$ Turbulence Models for Aerodynamic Flows," in *24th AIAA Fluid Dynamics Conference*, AIAA, 1993. AIAA Paper 93–2906.

[3] Hellsten, A. and Laine, S., "Extension of the $k-\omega$-SST Turbulence Model for Flows over Rough Surfaces," in *1997 AIAA Atmospheric Flight Mechanics Conference*, (New Orleans, Louisiana), pp. 252–260, Aug 1997. AIAA Paper 97–3577–CP.

[4] Menter, F. R., Kuntz, M., and Langtry, R., "Ten Years of Industrial Experience with the SST Turbulence Model," in *Turbulence, Heat and Mass Transfer 4* (Hanjalic, K., Nagano, Y., and Tummers, M., eds.), pp. 625 – 632, Begell House, Inc., June 2003.

[5] Spalart, P. and Rumsey, C. L., "Effective Inflow Conditions for Turbulence Models in Aerodynamic Calculations," *AIAA Journal*, Vol. 45, No. 10, 2007, pp. 2544–2553.

[6] Ala-Juusela, J. and Siikonen, T., "The Effect of Free-Stream Turbulence Parameters on the SST $k-\omega$ Turbulence Model, CFD/MECHA-20-2012," Aalto University, Department of Applied Mechanics, 2012.

[7] Rahman, M., Rautaheimo, P., and Siikonen, T., "Numerical Study of Turbulent Heat Transfer from a Confined Impinging Jet Using a Pseudo-compressibility Method," in *Proceedings of the 2nd International Symposium on Turbulence, Heat and Mass Transfer*, (Delft), pp. 511–520, June 1997.

[8] Siikonen, T., "Developments in Pressure Correction Methods for a Single and Two Phase Flow CFD/MECHA-10-2010," Aalto University, Department of Applied Mechanics, 2010.

[9] Langtry, R. B., *A Correlation-Based Transition Model using Local Variables for Unstructured Parallelized CFD codes*. PhD thesis, University of Stuttgart, Stuttgart, Germany, May 2006.

[10] Malan P., Suluksna, K. and Juntasaro, E., "Calibrating the $\gamma - Re_\theta$ Transition Model for Commercial CFD," in *47th AIAA Aerospace Sciences Meeting*, Jan 2009.